# Radiology

病人

　　陳先生，35 歲男性，某醫學中心急診部櫃台批價人員，在 2003 年 5 月台灣爆發 SARS（嚴重急性呼吸道症候群）期間，經常與緊急救護醫療網 (EMT）救護車隨從人員聊天，該 EMT 人員於一星期前被診斷為 SARS 入住負壓隔離病房治療。陳先生於兩天前開始出現發燒，畏寒，咳嗽，氣促等症狀，於是至發燒篩檢站就診。醫師詢問病史包括旅遊史，接觸史，臨床症狀等，診斷其為 SARS 疑似病例，Chest X-ray 影像發現病人右下肺葉有浸潤現象，因此高度懷疑為 SARS 可能病例，馬上安排入住負壓隔離病房接受隔離與治療。追踪一系列 chest X-rays，病人的肺部浸潤越來越嚴重，臨床上持續發燒，氣促及呼吸困難，病人的喉部拭子痰液檢體 RT-PCR 及 Real-time PCR 顯示 SARS Cov 陽性反應，因此診斷為 SARS 確定病例。在住院第 4 天接受插管及呼吸器治療。住院第 7 天因 ARDS（adult respiratory distress syndrome）及持續高燒不退，給予類固醇治療，入院第 10 天開始退燒臨床症狀獲得改善。第 14 天開始訓練脫離呼吸器，但 chest X-rays 有部分 fibrosis 變化，經物理訓練及呼吸照顧，病人終於不再依賴氧氣，而順利出院。
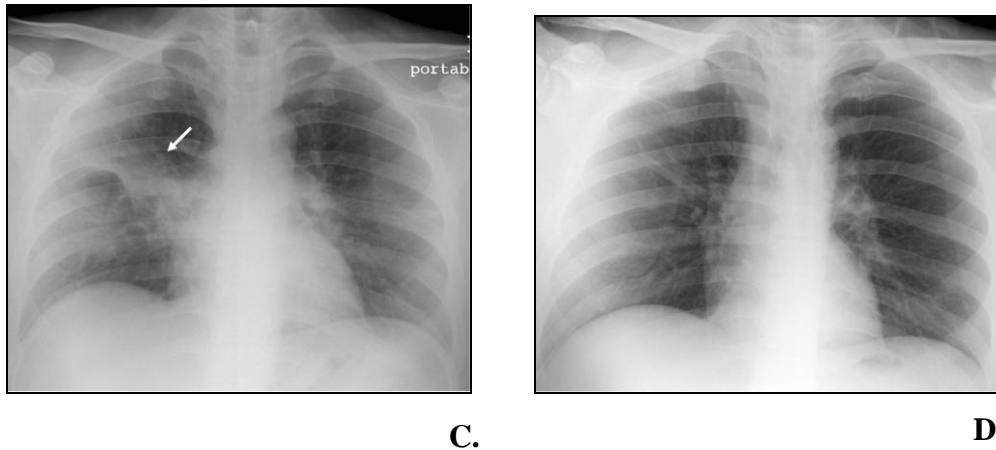

A.　　　　　　　　　　　　　　　　　　　　**B.**

C.   **D.**
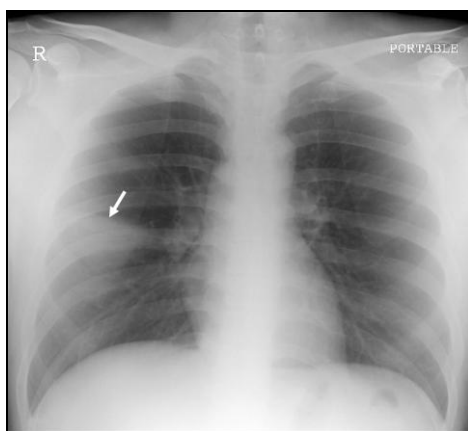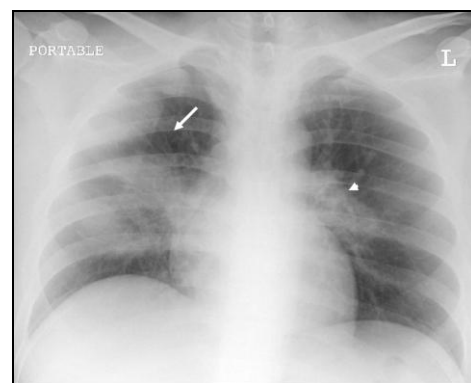
Fig. 1 (A) Initial chest PA film shows a patchy area of consolidation at right middle lung zone (arrow), consistent with pneumonia. **(B)** 7 days later, chest film reveals progressive alveolar infiltrates to right upper lung zone (arrow) and left perihilar region (arrowhead). **(C)** Chest X-ray obtained 9 days later shows regression of the infiltration at left perihilum and right upper lung zone (arrow). **(D)** After 19 days, chest film shows clear lung before discharge.

Questions:

1. What is the role of chest film in diagnosis of suspected patients with SARS?

2. What is the initial radiographic appearance of SARS?

3. Do radiographic patterns and distribution of pulmonary infiltration relate to clinical outcomes?

Learning objectives

1) To recognize appearance of initial chest radiographs in patients with SARS;

2) To recognize the role of radiologists in diagnosis and follow-up of patients with SARS and correlate these findings with clinical outcomes.

Discussion

Case Definitions (**revised 1 May 2003**) *for SARS by WHO (Radiology aspect)*

Diagnostic imaging has a major role in both diagnosis and categorization of SARS on the basis of case definitions issued by the World Health Organization and the Centers for Disease Control and Prevention. According to these case definitions, a *suspect* case is classified as a *probable* case when there are radiographic findings of pneumonia.

Suspect case   A person presenting after 1 November 2002 with history of: high fever (>38 ℃) AND cough or breathing difficulty AND one or more of the following exposures during the 10 days prior to onset of symptoms: close contact with a person who is a suspect or probable case of SARS; history of travel, to an area with recent local transmission of SARS; or residing in an area with recent local transmission of SARS.

Probable case   A *suspect* case with radiographic evidence of infiltrates consistent with pneumonia or respiratory distress syndrome on chest X-ray.

A *suspect* case with a normal CXR should be treated, as deemed appropriate, and monitored for 7 days. Those cases in whom recovery is inadequate should be re-evaluated by CXR. Clinicians are advised that patients should not have their case

放射線

definition category downgraded while awaiting results of laboratory testing or on the bases of negative results.

Initial chest radiographs

Chest radiography has a crucial role in the diagnosis and monitoring of disease progression in the treatment of patients with SARS. Frontal chest radiographs is obtained at initial clinical presentation (fever, 100%; dry cough, 54%, diarrhea, 19%) and once a day during treatment [1]. All initial chest radiographs is obtained after the onset of fever. Massive screening chest radiographs for suspected patients without fever is not recommended [1, 2]. However, attention should be given on the following patients without remarkable symptoms of fever: renal disease, DM, long-term steroid treatment, cancer, and immobile patients.

At the time of onset of fever, the initial chest radiographs show air-space opacification in 78 to 88% of patients with SARS [1, 3]. However, the initial radiographic appearance may be normal in febrile patients with SARS [1, 3]. The primary radiographic appearance of SARS can be air-space consolidation (69%), predominantly in the peripheral and lower lung zones, less common with ground-glass attenuation (8%), or uncommonly presenting with multiple bilateral nodules (4%). Pleural effusions have been uncommon (l5%) in previous reports [1]. Therefore, the presence of a pleural effusion does not exclude SARS.

CT scan is not recommended in screening *suspect* SARS patients.

Follow-up radiographs and patients' prognosis

There are four patterns of radiographic progression in SARS [3]; type 1 pattern (initial radiographic deterioration to peak level, followed by radiographic improvement with a maximum difference in overall mean lung involvement greater than 25%) is the most commonly observed and type 4 pattern (progressive radiographic deterioration)

seems to be associated with poor prognosis. In our experience, most patients in the recovery group showed the type 1 pattern and all patients in the group who died showed the type 4 pattern. The type 2 pattern (fluctuating radiographic changes) and type 3 pattern (static radiographic appearance) are less common.

In the recovery group, the worst chest radiographs developed at a mean of day 3 (range, day 1 to 8) [1]. The clinical outcome is better in younger patients and patients with initially normal lungs or a unifocal lung lesion. Progressive deterioration to diffuse unilateral or bilateral consolidation in the series of follow-up chest radiographs is associated with poor prognosis.

High resolution CT scan is more sensitive in detecting lung parenchymal change, such as fibrosis. Fibrosis, as detected by CT, has been reported to be presented in more than half (62%) of discharged patients with SARS. Therefore, high resolution CT scan is recommended as a baseline sensitive imaging in follow-up recovery patients before discharge from hospital.
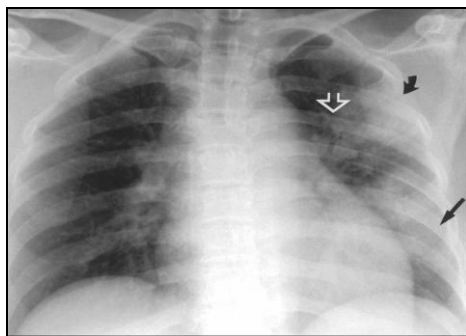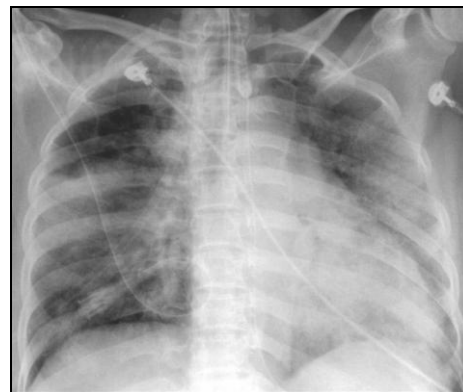
A.   **B.**

Fig. 1.—29-year-old previous healthy woman who presented with fever and dry cough. (**A**) Initial chest radiograph shows air-space consolidation in left lung. Upper (curved arrow), middle and lower (arrow) lung zones and both medial (open arrow) and lateral compartments are involved. (**B**) Chest radiograph obtained 15 days later shows progression of disease and bilateral consolidations, predominant in right middle, left middle and left lower lung zones, consistent with clinical diagnosis of acute respiratory distress syndrome.
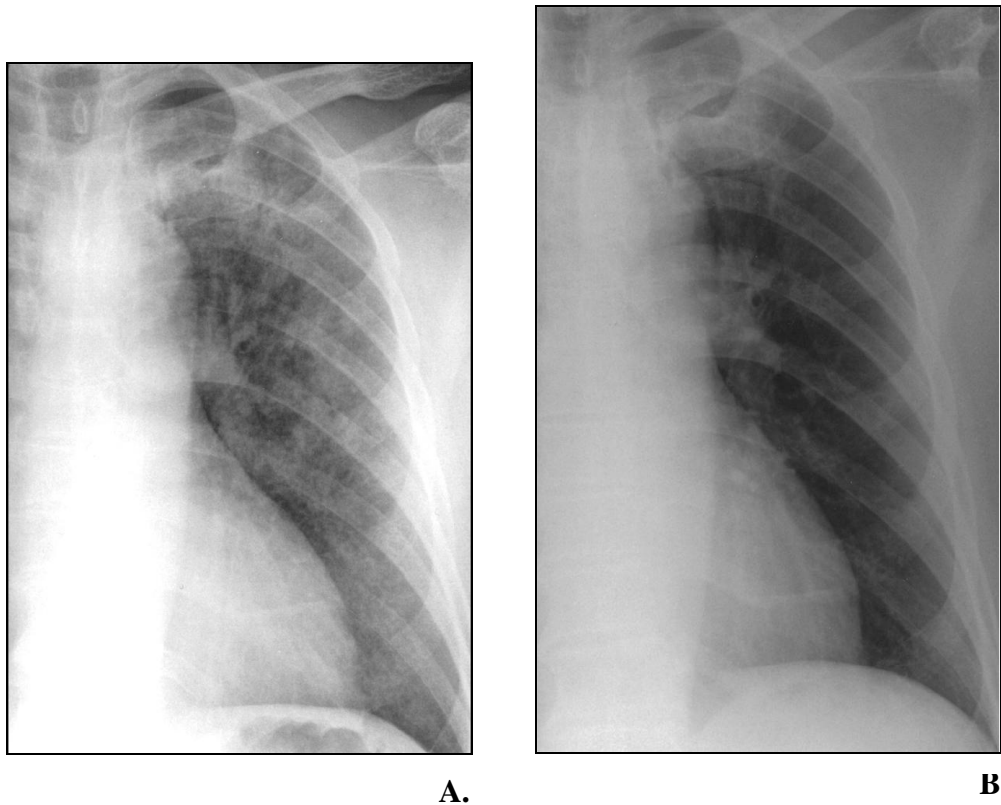
Fig. 2. —59-year-old man who presented with fever, dyspnea and chest pain. (**A**) Initial chest radiograph shows ground-glass attenuation in left upper, middle and lower lung zones. (**B**) Chest radiograph obtained 4 days after initial film. Left middle and lower lung zones have cleared and residual ground-glass attenuation is noted in left upper lung zone.

Fig. 3. —90-year-old man who presented with fever, dry cough and leukopenia. Frontal chest radiograph shows areas of consolidation bilaterally in lower lung zones and bilateral pleural effusions (arrows).
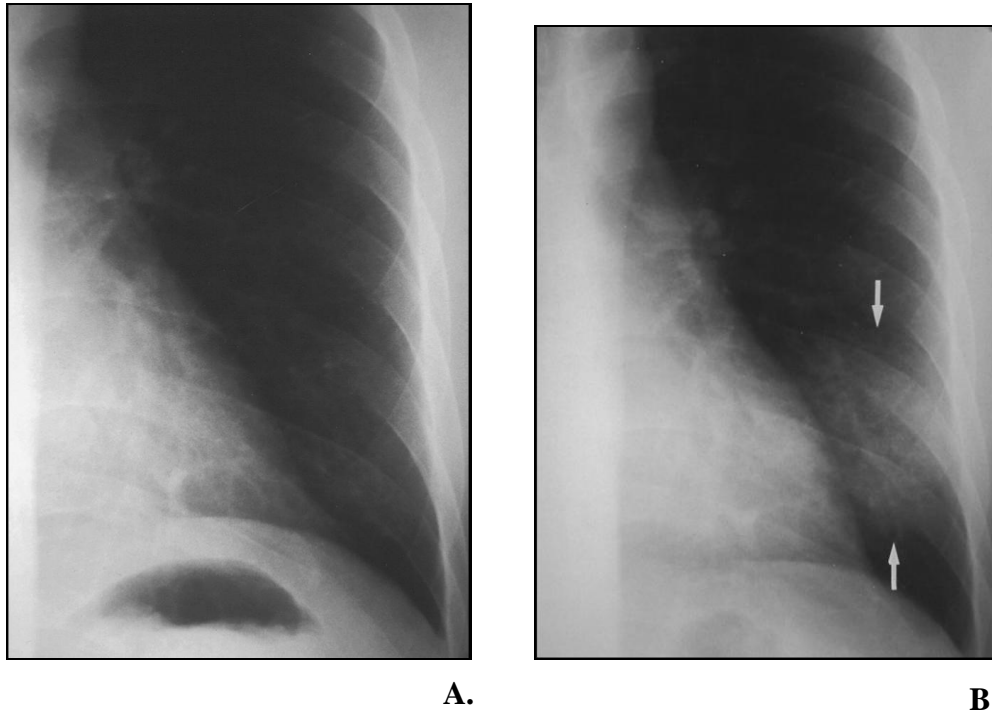
A. **B.**

Fig. 4.—31-year-old man who presented with fever, chills, cough and diarrhea. (**A**) Left lower lung zone on initial chest radiograph is normal. (**B**) Chest radiograph obtained three days after initial symptoms shows air-space consolidation at left lower lung zone (arrows).

Radiographic patterns and histology

SARS is a form of lung injury characterized by epithelial-cell proliferation and an increase in macrophages in the lung. In patients with SARS of duration less than 10 days, there is hyaline-membrane formation, pneumocyte proliferation, and edema. Diffuse alveolar damage is seen in cases of longer duration. The diffuse alveolar damage typically goes through an exudative phase followed by a proliferative phase [4]. Pulmonary edema with hyaline membrane formation occurs in early alveolar damage, and is then followed by cellular fibromyxoid exudates in air spaces. These findings may be identical to the rapidly progressing bilateral ground-glass opacifications or consolidations observed in some of our patients as well as patients in other series [6] that are consistent with acute respiratory distress syndrome.

Differential diagnosis

The radiographic appearances of SARS are nonspecific and may be

indistinguishable from those of bacterial bronchopneumonia or viral infections, and they share CT features with other conditions that result in subpleural air-space disease, such as bronchiolitis obliterans organizing pneumonia and acute interstitial pneumonia. In later stages, particularly with diffuse involvement of the lungs, the radiographic appearance is similar to that of acute respiratory distress syndrome.

Other emerging infectious disease—Avian Influenza A (H5N1)

Published information about clinical course of Avian Influenza A infection is limited. In 1997 Hong Kong outbreak, patients developed symptoms with fever, sore throat, cough, and lymphopenia, carries a high risk of death. It is believed that most cases of Avian Influenza A infection have resulted from contact with infected poultry or contaminated surfaces.

Although patients with exposure to ill poultry and severe pneumonia, or patients with exposure and laboratory evidence of influenza A infection not confirmed as H5N1.

Chest radiographs have been reported to be all abnormal on patients' admission to hospital [5]. In Thailand (2004) report [5], all 12 patients had abnormal chest radiographs with a median of 7 days after onset of fever (range 3–17 days). Two patients had interstitial infiltration, and 10 had patchy lobar infiltrates in a variety of patterns (single lobe, multiple lobes, unilateral or bilateral distributions). The radiographic pattern progressed to diffuse bilateral ground-glass appearance, with clinical features compatible with ARDS, in all 8 patients who died and in 1 patient who survived. The median time from onset to ARDS development was 6 days (range 4–13). Similar radiographic appearance for H5N1 infection in 10 patients in Vietnam was also noted [6]. There were no pleural effusions.

References

1. Hsieh SC, Chan WP, Chien JC, Lee WS, Yao MS, Choi WM, Chen CY, Yu C. Radiographic appearance and clinical outcome correlates in 26 patients with severe acute respiratory syndrome. AJR Am J Roentgenol 2004;182:1119-1122

2. Chan WP, Liao YM. "SARS Infection Control Guidelines for Radiology Department": An example from Taipei Medical University－Municipal Wan-Fang Hospital. Chinese Journal of Radiology 2003; 28: 167-173

3. Wong KT, Antonio GE, Hui DSC, et al. Severe acute respiratory syndrome: radiographic appearances and pattern of progression in 138 patients. Radiology 2003; 228: 401-406

4. Nicholls JM, Poon LM, Lee KC, et al. Lung pathology of fatal severe acute respiratory syndrome. Lancet 2003;17:1773-1778

5. Chotpitayasunondh T, Ungchusak K, Hanshaoworakul W, et al. Human disease from influenza A (H5N1), Thailand, 2004. Emerg Infect Dis 2005; 11: 201-209.

6. Hien TT, Liem NT, Dung NT, et al. Avian influenza A (H5N1) in 10 patients in Vietnam. N Engl J Med 2004; 350: 1179-1188.

Radiology

放射線

Learning objectives

1) To recognize radiological signs of HCC and tumor rupture;

2) To recognize the role of radiologists in diagnosis, treatment and follow-up of patients with HCC.

Case Presentation

A 50-year-old man was a hepatitis B carrier for decades and also was a heavy drinker for many years. He had fatty liver but he never follow up his liver problems. In this admission, he was brought to our emergent department at night due to sudden onset of abdominal pain, cold sweating, and dizziness. He mentioned that he had nausea and dull pain over upper abdomen in the afternoon, and the sensation turned to sharp pain with cold sweating about 3 hours before. No fever or passage of tarry stool was noted. He denied systemic diseases or history of gastric ulcer, or trauma.

On clinical examination, his consciousness was clear and vital signs were stable, except tachycardia. Blood pressure measured 102/60mmHg. His abdomen was soft and flat with mild tympanic, and no hepatosplenomegaly. Epigastric tenderness was noted, and some degree of shifting dullness over the abdomen. Bowel sound was diminished. Laboratory data revealed elevated liver function (GOT: 134; GPT: 89) but alfa-fetoprotein was normal (AFP: 19.0ng/ml). Hepatitis markers revealed positive HBsAg and negative Anti HCV. Prothrombin time was 1.9sec [control: 12.4].

Emergent CT scan was performed and precontrast images showed fatty infiltration of the liver. High-density fluid was noted at perihepatic space and left

subhepatic space and accumulation in the peritoneal cavity (Fig. 1A). On postcontrast images, a soft-tissue density mass, measured 5.5cm in diameter, was detected at lateral segment of left lobe of the liver (Fig. 1B). Disruption of the capsule was noted. There was no lymph node enlargement or abnormal collateral vessels. The portal vein was patent. CT findings were compatible with ruptured hepatocellular carcinoma (HCC) and hemoperitoneum.
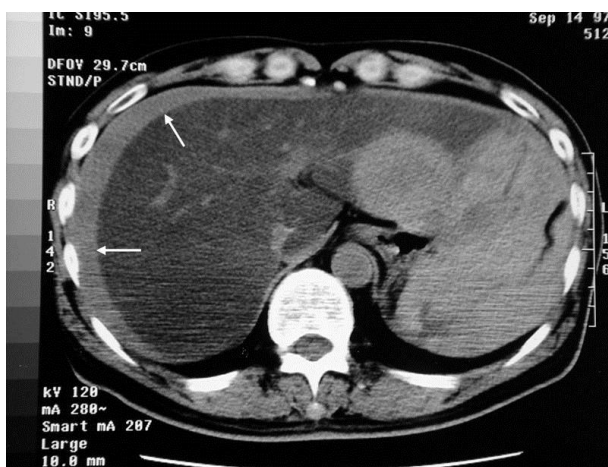

Fig. 1A. Precontrast CT image shows high-density fluid (arrows) surrounding perihepatic space due to hemoperitoneum. The liver parenchyma revealed lower density than the spleen, indicating fatty liver. A well-defined tumor at left-lobe liver is noted.

Fig. 1B. Postcontrast CT image shows that the perihepatic fluid turns to isodensity relative to the liver. The tumor has an enhancing capsule with a suspected rupture site (arrow) at its posterior portion.

As suggested by the surgeon, emergent transhepatic arterial embolization (TAE) was performed for this patient. Celiac arteriogram showed a solitary hypervascular mass with neovascularity and tumor stain at left lobe of the liver (Fig. 1C). TAE was performed with catheter tip at the left hepatic artery and gelfoam cubes, following stripes, were injected. Post-embolization proper hepatic arteriogram revealed complete obliteration of the tumor vessels.
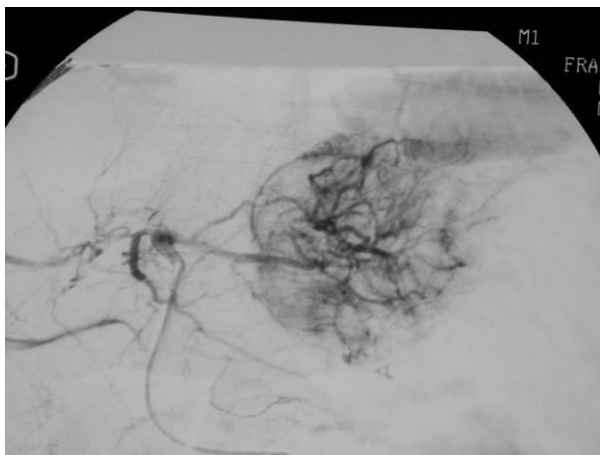

Fig. 1C. Celiac arteriogram shows a hypervascular tumor with neovascularity at left lobe of the liver.

The patient was later received left lateral segmentectomy of the liver. Histology of the specimen revealed HCC.

Discussion

CT patterns and histology

General concepts: A routine CT scan of the liver obtained from a spiral CT scan includes precontrast images (Fig. 2A), and postcontrast arterial and venous

phase images. Arterial phase images can be seen with obvious enhancement of aorta (Fig. 2B) and renal cortex, while venous phase images can be identified with enhancement of IVC (Fig. 2C) and renal medulla. A normal liver usually has about 7HU higher density than that of the spleen that can be recognized by our eyes. Fatty liver usually has lower density as compared with the spleen on *precontrast* images. Acute or subacute hemorrhage in the peritoneum usually has higher density that that of water density or even soft-tissue density. For water density, we may use bile in gall bladder for reference, and for soft tissue, density of spleen is an appropriate internal control.

Fig. 2A. Precontrast CT image show coarse liver parenchymae, suggesting some degree of liver cirrhosis.
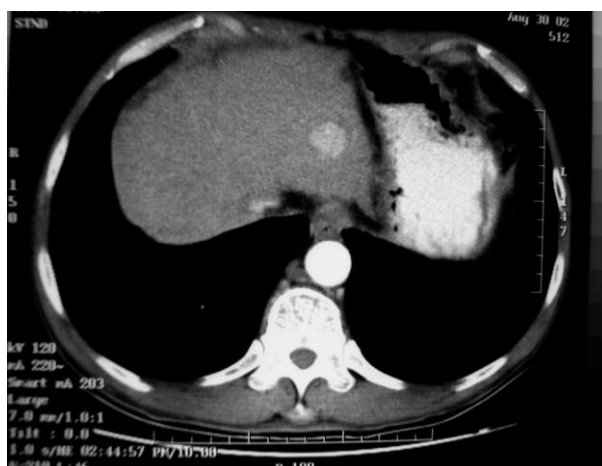
Fig. 2B. Postcontrast arterial phase image shows an enhancing nodule at left lobe of the liver. A hypervascular tumor, such as HCC, is most likely. Note that the aorta is markedly enhanced in this arterial phase.

Fig. 2C. Postcontrast venous phase image shows wash-out effect of the nodular enhancement.

Vascular tumors of the liver, such as HCC or metastasis, that receive most of their functional blood supply from the hepatic arterial flow will enhance the tumors during the arterial phase on CT images [Baron 2004]. In contrast to hypervascular tumors, hypovascular tumors (such as hypovascular metastasis) are visualized optimally during the portal venous phase, which is the time of maximal normal liver enhancement and minimal tumoral enhancement. Normal hepatic parenchymae receive most of their nutrient blood from portal veins and, therefore, will be enhanced during the venous phase. However, small percentage of small HCCs that are hypovascular, portal venous phase imaging will be the optimal phase of contrast enhancement for tumoral detection [Baron 2004].

On the contrary, hepatic hemangiomae commonly show progressive enhancement, from periphery to central, from arterial phase to venous and delayed phase images (Fig. 3).
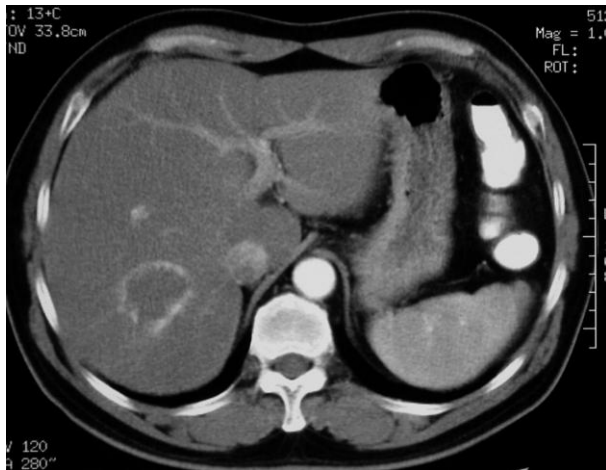

Fig. 3A. Hepatic hemangioma. Arterial phase CT image shows a peripheral enhancement of a tumor mass at posterior segment of right hepatic lobe. Note that the aorta is marked enhanced.
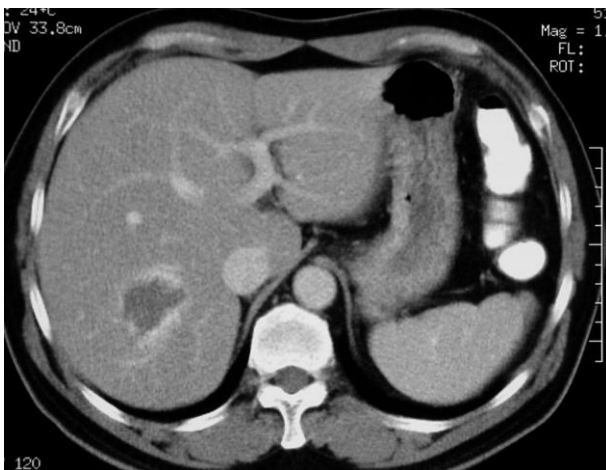

Fig. 3B. Venous phase CT image shows progressive enhancement from periphery of the hepatic mass. Note that equilibrium of contrast enhancement in the aorta and IVC.

Fig. 3C. Venous phase CT image (lower cut) shows mural enhancement from periphery to central part of the hepatic mass.
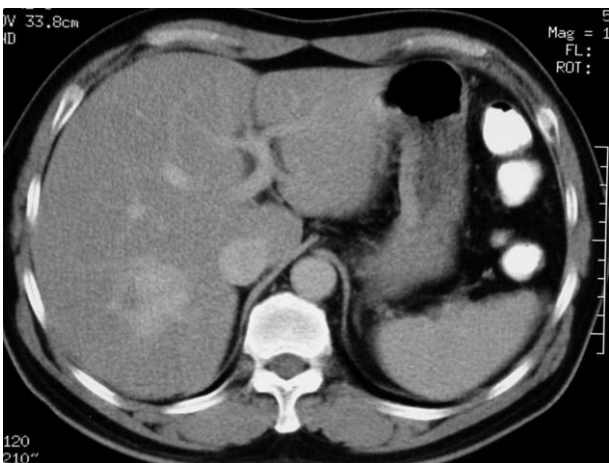

Fig. 3D. Delayed phase CT image shows pooling of contrast medium into the central part of the hepatic mass. Hemangioma is compatible.

Besides, a complete interpretation of HCC should include aortocaval space for lymphadenopathy, ascites or collateral vessels for liver cirrhosis, hemoperitoneum for tumor rupture, portal vein and IVC for tumor thombosis, and of course the tumor margin, size, location and number of tumor masses. These findings are helpful for planning of further treatment.

Transhepatic arterial chemoembolization (TACE)

Methods: Chemoembolization for HCC is performed following selective catheterization of the right or left hepatic artery, or occasionally the superior mesenteric artery (SMA), depending on the supplying artery of the tumor. Protocols vary among medical centers, but all involve delivery of one or more chemotherapeutic agents (e.g., doxorubicin, cisplatin, and mitomycin C) suspended in water-soluble contrast and iodized oil, which acts as a carrier for the chemotherapeutics and slows blood flow. Particulate embolization, most commonly in the form of gelatin foam (Gelfoam) slurry, is performed during the same session. The main principle for chemoembolization is near-stagnation of blood flow in the arterial distribution of the targeted lesion(s). Postprocedural hospital admission may range from 2 to 5 days. Follow-up CT scan is optimally performed in 4 to 6 weeks after TACE treatment.

Complications: Pain, fever, nausea, vomiting, leukocytosis, and transient elevation of liver enzymes are, in brief, the postembolization syndrome. Supportive therapy typically suffices. Major complications may occur in 3% to 4% of patients and include hepatic failure, hepatic infarction, hepatic abscess, tumor rupture, hepatic arterial occlusion, and nontarget embolization.

Patients' prognosis: The efficacy of TACE is controversial. In sizable series, survival rates at 3 years have ranged from 13% to 40%. Although some investigators have found no survival benefit of TACE over symptom treatment, two European groups demonstrated a survival benefit for patients with unresectable HCC treated with TACE versus those not treated. The 3-year survival rates of treated patients were 26% to 27% versus 3% to 5% for the untreated patients.

Because HACE cannot achieve the survival rate of patients undergoing surgical resection for HCC, it should be reserved for patients with unresectable HCC.

Contraindication: TACE should not be performed in patients with predominant or extensive extrahepatic disease. Because TACE, unlike ablation, causes some damage to the hepatic parenchyma not involved with tumor, significant baseline liver dysfunction is a contraindication. Refractory ascites and difficult-to-control encephalopathy are also associated with a greater risk for postprocedural hepatic failure. Biliary obstruction with intrahepatic ductal dilatation is a contraindication to TACE because of an associated high risk for biliary necrosis. Portal vein occlusion is a relative contraindication.

References

1. Baron RL, Brancatelli G. Computed tomographic imaging of hepatocellular carcinoma. Gastroenterology 2004 Nov; 127(5 Suppl 1): S133-43

Radiology

病　　人

林女士，<u>65 歲，女性</u>，是一個在丘陵地務農的原住民農婦，體型肥胖，經常負重的工作或長時間的站立爬坡，兩膝疼痛，膝活動受限已困擾了這位農夫十五年了，初期主訴兩膝疼痛、上下坡費力、彎曲受限、蹲下困難，經病史、理學檢查及<u>平面 X 光診斷為初期關節炎 (Fig. 1)</u>。經保守治療，包括 NSAID 藥物、肌肉鬆弛劑、關節注射玻尿酸、局部使用 steroid（類固醇）及軟骨再生藥物(glucosamine, Chondroitin)、復健治療(肌力訓練、紅外線超音波治療)等，也接受衛教觀念(運動、減肥、飲食教育、工作改變等)，病狀雖有改善，但仍時好時壞，常有關節 ”卡住” 或 ”鬆脫” 的症狀後，經 <u>MRI 檢查診斷為骨性關節炎後之關節面初期磨損及半月軟骨損傷 (Fig. 2)</u>，也接受了關節鏡的檢查及關節沖洗清創術及關節面刮平、滑膜刨削術、半月軟骨部分切除手術。

術後，經歷了十五年的症狀減輕下，由於農婦的勤奮個性，不忘務農本業，繼續粗重工作，六十五歲時，後續追踪，兩膝關節嚴重變形，膝內翻及履次關節積水，無法上下坡，走 100 公尺必須多次休息，需拐杖助行，X 光顯示：<u>膝關節的三大部份關節軟骨完全破壞、關節面狹窄、退化性骨刺、游離體及變形、軸位改變 (Fig. 3)</u>。經骨科醫師診斷：嚴重退化性骨關節炎併膝內翻 (OA with Genus Varus)，保守治療無效。醫師建議行兩膝關節重建手術，行兩膝全人工關節置換術 TKR (Total Knee Replacement)，術後加強復健衛教，目前已恢復正常走路無疼痛，不需枴杖或助行器。

Learning objectives

1. To be familiar with the radiologic findings of osteoarthritic knee.

2. To understand the role of MR imaging in diagnosis of osteoarthritic knee in selected patients.

Questions

1. What criteria can be used for diagnosis of osteoarthritic knee on plain radiographs?

2. What further studies can be used to obtain the diagnosis of early osteoarthritic knee in selected patients for potential aggressive treatment?

3. How do you monitor the progression of osteoarthritic knee?

Teaching guides

Osteoarthritis of the knee is one of the most prevalent and disabling chronic conditions affecting older adults. Diagnosis of osteoarthritic knee is primarily based on history and physical examination, but radiographic findings are helpful when diagnosis is uncertain. The radiographic hallmarks of osteoarthritic knee are asymmetric joint space narrowing (predominant, medial tibiofemoral compartment) (Figures 3 and 4), subchondral sclerosis, osteophyte formation, subchondral cysts, and eventual subluxation follow. The distribution patterns of osteoarthritic changes also are helpful to address the diagnosis. Osteoporosis and erosions are not usual features of this disease.

X-rays can help in the diagnosis and may be the only special test required in the majority of cases. X-rays can also help doctors rule out other problems, since knee pain from OA may be confused with other common causes of knee pain, such as a torn meniscus or kneecap problems. In some cases of early osteoarthritis, X-rays may not show the expected changes. Therefore, a negative X-rays cannot exclude early OA knee.

Radiographic JSN is not a reliable tool for assessing cartilage status in patients with early osteoarthritis or in chronic knee pain. Severity of joint pain can be used to predict subsequent JSN or as a indicator for operation. X-rays are only an indirect measure of cartilage loss. Magnetic resonance imaging (MRI) provides a more direct image of cartilage as well as what is going on throughout the joint tissues and now is being tested as a tool for monitoring small

changes in cartilage over time (Figures and 5 and 6). Prevalence of meniscal tears is high in older people with osteoarthritic knee. A previous report has indicated that a medial meniscal tear was detected in 86% of patients with symptomatic osteoarthritis of the knee. Meniscal subluxation is a common finding in patients with osteoarthritis of the knee, and increasing meniscal subluxation has been correlated with the severity of JSN.

Structural morphological changes on X-rays are also considered the primary outcome variables for assessing the progression of OA. The development of new methods for prevention and treatment of OA requires improved understanding of the factors that influence its progression. The ability to assess progression quantitatively is a necessary first step in understanding factors that influence the disease process. Depending on the joint studied, several indices are currently used for assessing radiological progression of OA, including individual radiographic features (e.g., marginal osteophytes), composite indices (e.g., Kellgren and Lawrence scoring systems) (Table 1), and quantitative measures (e.g., joint space width measurement). However, the longitudinal rate of JSN indicates that the yearly change may be very small and of doubtful clinical significance. More than 50% of the patients with reductions in the joint space width at 1 and 2 years had no loss of cartilage volume.

Table 1.   Kellgren and Lawrence scoring systems assessment of radiological progression of osteoarthritic knee

Kellgren-Lawrence	Definition
Grade 0	No features
Grade 1 (Doubtful)	Minute osteophyte, doubtful significance
Grade 2 (Minimal)	Definite osteophyte, unimpaired joint space
Grade 3 (Moderate)	Moderate diminution of joint space
Grade 4 (Severe)	Joint space greatly impaired, with sclerosis of subchondral bone

Current report indicated that MRI can detect interval cartilage loss in patients over a short period (<2 years). The presence of meniscal and ACL tears was associated with more rapid cartilage loss. Cartilage lesions located in the central region of the medial compartment showed more rapid progression of cartilage loss than cartilage lesions in the anterior and posterior portions of the medial compartment

Findings:

1. degenerative changes

- osteophyte from superior aspect patella

- osteophytes from anterior aspect of femoral condyles

- small lateral osteophyte from lateral femoral condyle

- small medial osteophyte from medial tibial plateau

- decrease in height of medial femoro-tibial compartment

- early sclerosis and remodelling of medial femoro-tibial compartment articulating surfaces
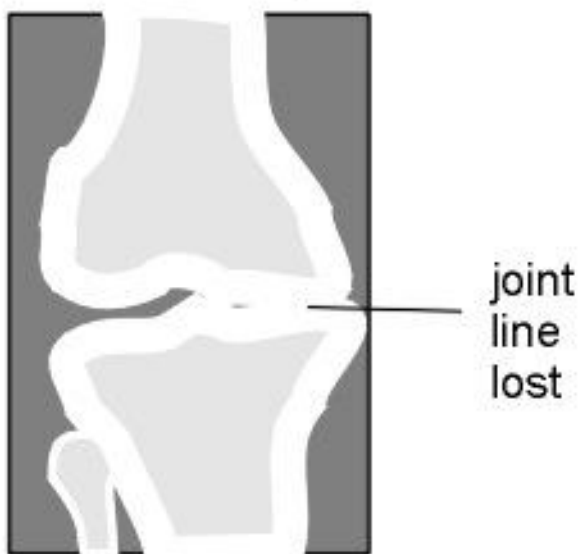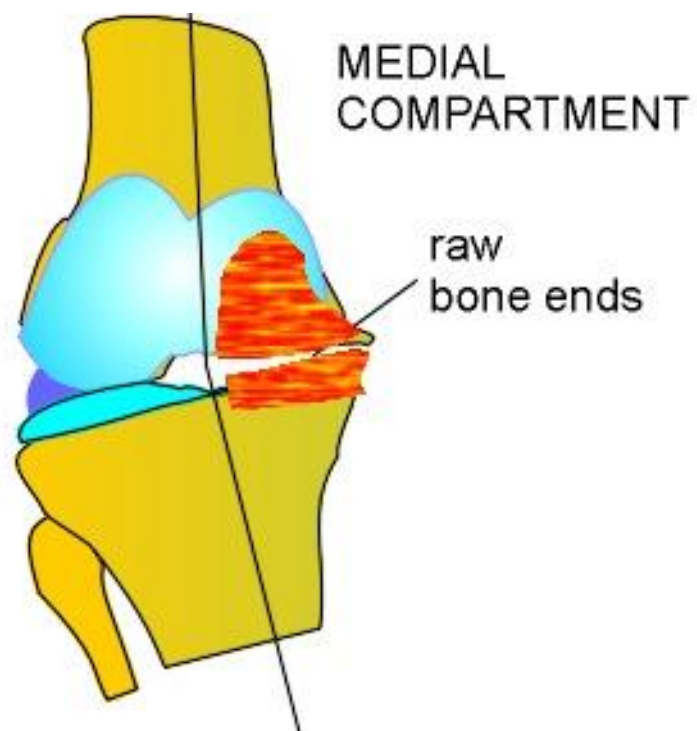
Figure 1.

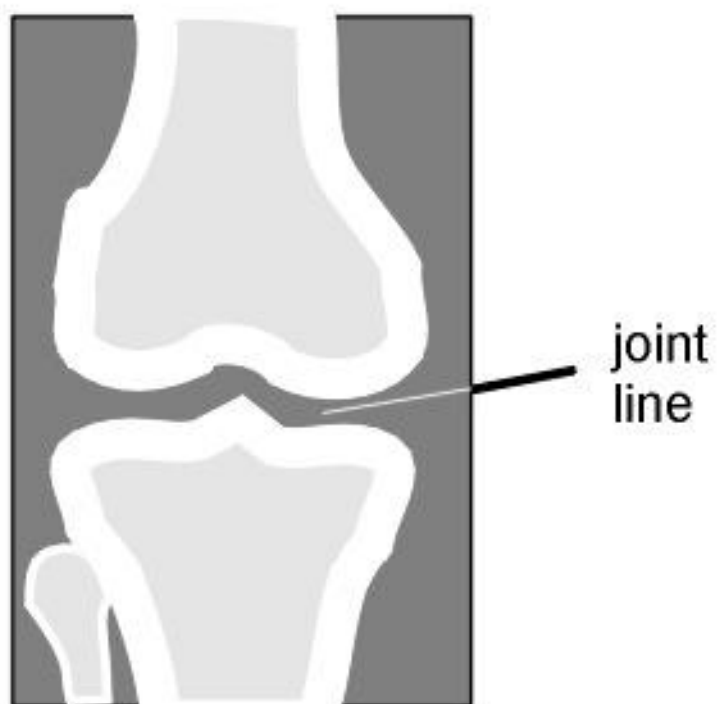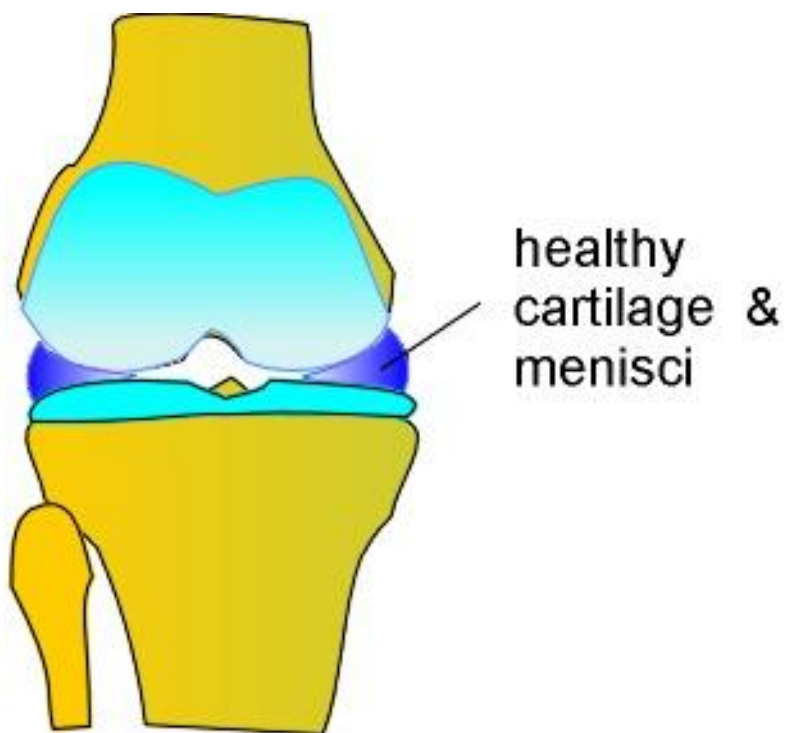**Figure 3.   63 y/o male with chronic knee pain.**

Diagnosis: Osteoarthritis with meniscal degenerative tears, cartilage loss and associated marrow edema. Large popliteal cyst with loose body.

Figure 4.   55y/o female with chronic knee pain.

Diagnosis: Osteoarthritis(lateral and patellofemoral compartments) with cartilage loss and intra-articular loose bodies.

MEDIAL
COMPARTMENT

raw
bone ends

joint
line
lost

X RAY PICTURE
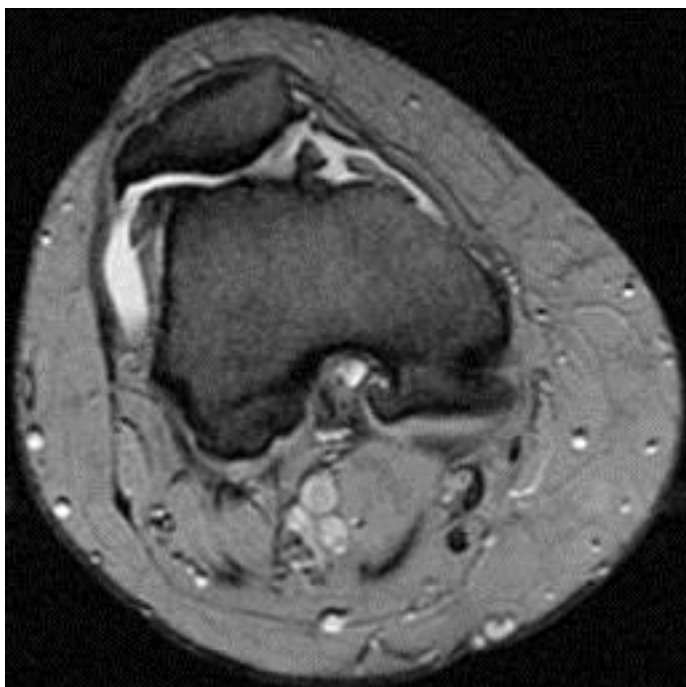
healthy
cartilage &
menisci

joint
line

X RAY PICTURE

放射線

References

1. Biswal S, Hastie T, Andriacchi TP, Bergman GA, Dillingham MF, Lang P. Risk factors for progressive cartilage loss in the knee: a longitudinal magnetic resonance imaging study in forty-three patients. Arthritis Rheum. 2002 Nov;46(11):2884-92.

放射線

RADIOLOGY

Learning objectives

1. To learn basic concepts of dual energy X-ray absorptiometry (DXA) in assessing body composition;

2. To learn impact of radiologic exam. in obese patients

The Patient

廖先生四十歲已婚，研究所畢業，科技公司高級工程師。有兩個在唸小學的兒女。大學時身高號稱 180、體重 75 公斤是運動好手，自從當兵退伍進入工作職場以後，因為工作壓力大且常常加班熬夜，偶而還要應酬喝酒，加上沒有規律運動，體重逐漸增加，最重曾經達到 100 公斤，後來自己力行運動及飲食控制，加上接受藥師朋友建議吃過一個月減肥藥，體重控制在 95 公斤上下。家族史中，父親有糖尿病及高血壓，因腦中風過世，母親有高血脂症接受規則服藥控制。

近半年出現容易疲勞，尤其到下午四、五點時精神最差，開會中常會打瞌睡，工作效率也因此變差；公司例行性檢查發現有脂肪肝、高血壓、高血脂症狀，因此建議到醫院進一步檢查，門診檢查身高 178 公分、體重 98 公斤、身體質量指數(BMI) 30.9、腰圍 102 公分，

安排雙能量 X 光檢查(DXA)發現身體脂肪比例超過 40%，廖太太也抱

怨先生晚上睡覺時鼾聲大作，還不時出現呼吸停止現象，減肥門診醫

師建議廖先生進一步接受睡眠、生化及內分泌檢查，此外也建議他開

始積極減重，包括規律的運動、低熱量飲食，減少坐式生活方式、少

吃宵夜、多吃蔬菜水果等。三個月後，體重下降至 93 公斤，但出現

停滯現象，除了建議他繼續減重外，也給予合法減肥藥，希望他至少

減到 88 公斤。

Questions

1. How does DXA measure body composition?

2. How do you define obesity and fat distribution based on DXA
   measurement?

3. What is the impact of body habitus on radiologic imaging quality?

Teaching guide

Principal of DXA in measuring body composition

Dual energy X-ray absorptiometry (DXA) can estimate three body
compartments consisting of fat mass, lean body mass, and bone mass.
DXA systems use a source that generates X-rays at two energies. The
differential attenuation of the two energies is used to estimate the bone
mineral content and the soft tissue composition. When two X-ray
energies are used, only two tissue compartments can be measured;
therefore, soft tissue measurements (i.e., fat and lean body mass) can only

be measured in areas where no bone is present. DXA also has the ability to determine body composition in defined regions, such as the arms, legs, and trunk. DXA measurements are based in part on the assumption that the hydration of fat-free mass remains constant at 73%. Hydration, however, can vary from 67%–85%, and can be variable in certain disease states. Other assumptions used to derive body composition estimates are considered proprietary by DXA manufacturers (e.g., Lunar, Hologic, and Norland).

The fat content is given in percentage. DXA device are proven to have long-term stability and high precision in body composition scans of 2 to 6%.

DXA body composition studies have emerged as a potential new reference standard for body studies, replacing underwater weighing. DXA measurements of body mass continue to be included as outcomes measures in various trials, frequently focusing on HIV-associated lipodystrophy. However, while DXA scans have become a valued research tool, it is unclear how information regarding body composition could be used in the active medical management of the patient to improve health outcomes.

It has been well documented that too much body fat, especially when located around the abdomen, increases the risk of many diseases, including type II diabetes, high blood pressure, stroke, heart disease, and certain cancers.

Definition of overweight and obese

Determines underweight (<18.5), normal weight (18.5-24.9), overweight (25.0-29.9), and obese (30.0 – 39.9) based on a person's height and weight. A result greater than 40 is considered morbidly obese, which can be a potentially deadly situation.

Individuals with a BMI of 25 to 29.9 are considered **overweight**, while individuals with a BMI of 30 or more are considered **obese**.

Waist-to-hip ratio (WHR)

Waist-to-hip ratio (WHR) is the ratio of a person's waist circumference to hip circumference, mathematically calculated as the waist circumference divided by the hip circumference. For most people, carrying extra weight around their middle increases health risks more than carrying extra weight around their hips or thighs. (NOTE: Overall obesity is still more risky than body fat storage locations or waist-to-hip ratio.)

Undesirable waist circumferences differ for men and women.

- Men are at risk who have a waist measurement greater than 40 inches (102 cm)

- Women are at risk who have a waist measurement greater than 35 inches (88 cm)

Generally, men with more than 25% body fat and women with more than 30% are considered obese.

Measurement of fat distribution

a. Pear Obesity (gynoid Obesity)

b. Apple Obesity (android Obesity, beer belly)

Higher cardiovascular disease risk

Higher risk of Insulin Resistance

c. Values suggestive of Apple Obesity

Males > 1.0 confers increased risk

Females > 0.9 confers increased risk

For both men and women, a waist-to-hip ratio of 1.0 or higher is considered "at risk" or in the danger zone for undesirable health consequences, such as heart disease and other ailments connected with being overweight. When w/h exceeds 1.0 in men or 0.9 in women, one can speak of central obesity.

Android

Gynoid
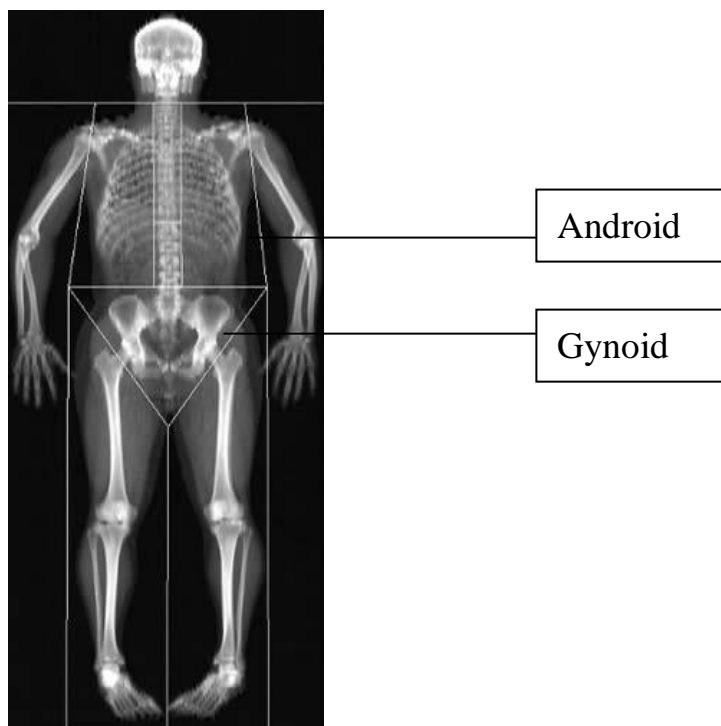
Limitation of DXA

DXA (a two-compartment method) does not measure body water, which limits its accuracy in body composition assessment. In overweight subjects, overlapping of body parts may affect the total results due to increased thickness in overlapping regions.

Impact in imaging obese patients

Obesity presents many challenges in health care. In addition to increasing risk for the development of chronic disease, obesity is a limiting factor in radiology used in all aspects of medical diagnosis and treatment. These limitations include both logistical and image quality issues. Large body habitués also degrades image quality, making it difficult or impossible to obtain adequate images for clinical interpretation

Ultrasound: In an obese patient with 8cm of extra-peritoneal fat, there would be about 6% of the original beam intensity or a 24 dB drop in sound level before the beam enters the peritoneal cavity. Attenuation is less at lower frequencies but results in decreased image resolution.
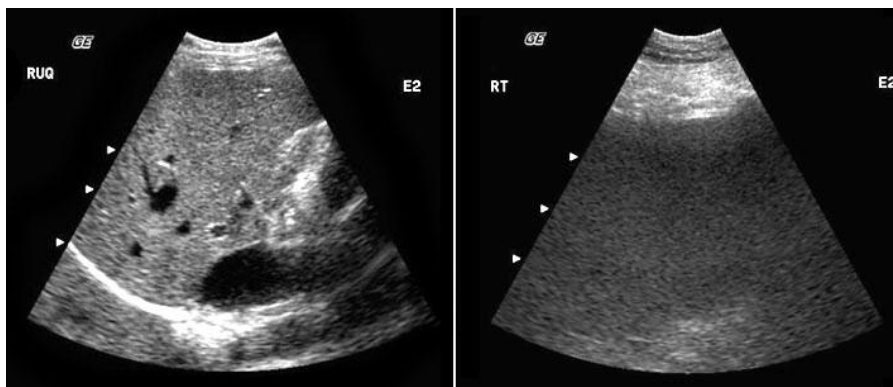
X-rays: Image quality on plain radiographs is also severely limited by attenuation. Increasing the current and exposure time can improve image quality but also increases the radiation dose to the patient and cause motion artifact due to increased exposure times.
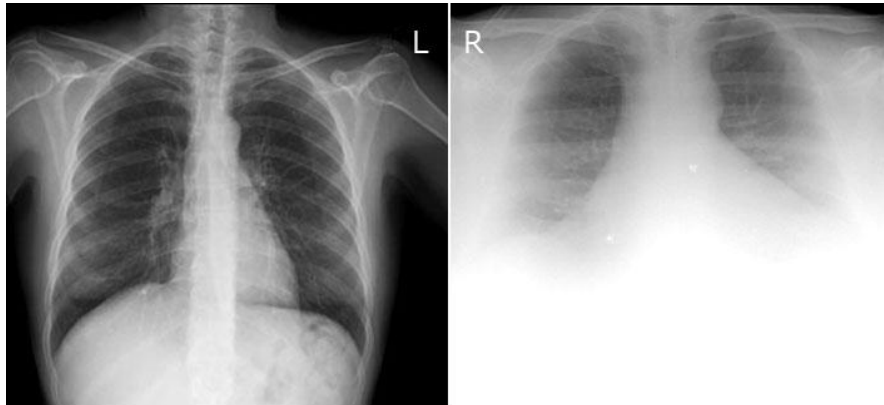
CT scan: X-ray attenuation also limits image quality for CT images, although to some degree attenuation can be compensated for by increasing the tube current and decreasing the rotation speed of the gantry.
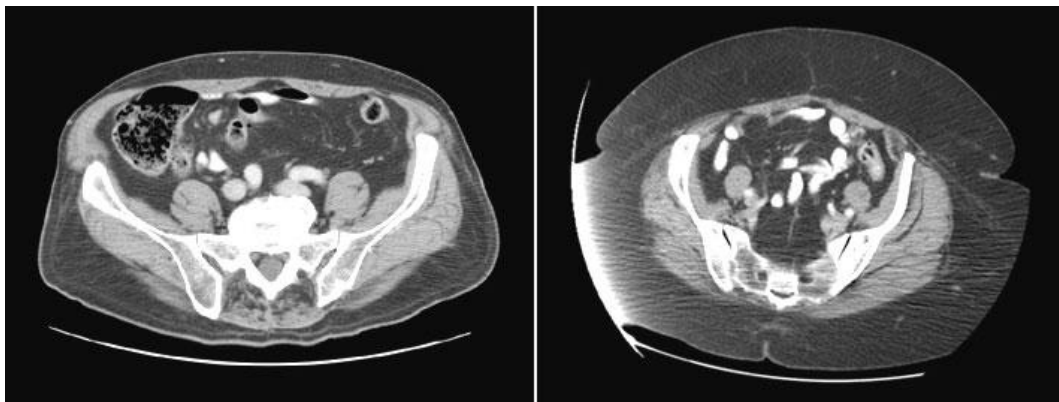
1. Whole Body Dual X-Ray Absorptiometry (DEXA) to Determine Body Composition. www.regence.com/trgmedpol/radiology/rad41.html
2. MGH Radiology Grand Rounds Newsletter. Radiology Rounds - July 2005 - Imaging and Obese Patients.

醫學系放射學科 陳榮邦

Radiology

Learning Objectives:

1. To be familiar with the imaging evaluation of patients with epilepsy.

2. To understand the role of CT scan and MRI images in diagnosis of patients with epilepsy.

Case presentation:

　　一個 64 歲男性病人任職某建築公司，最近一個月內有 3 次意識障礙伴隨四肢抽搐而就醫。發作時，他只記得右下肢重複抽動 5 分鐘，而他的妻子發現他有眼睛上吊、咬舌頭及四肢抽搐之症狀約 10 至 20 分鐘，半小時之後，他的神智恢復正常。在最近一年他發現他的右下肢較為僵硬，且右手的動作也較不靈活。

　　神經學檢查發現右上肢及右下肢有輕度肌力減退，右側肢體深部肌腱反射增加，且右下肢有陽性 Babinski 徵候，其他神經學檢查為正常。頭部電腦斷層發現在左側蝶骨樑（sphenoid ridge）長出一顆界限清楚、有顯影的腫瘤。
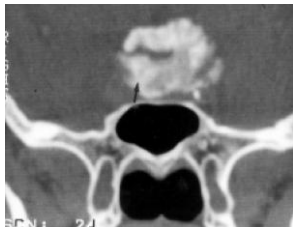
Coronal CT scan of the brain (Bone Window) showing the calcified sphenoid ridge meningioma (arrow)

Questions:

1. What's role of CT or MRI in evaluation of patients with epilepsy?

2. What findings are seen on CT or MRI in patients with epilepsy?

Teaching guides:

Medial sphenoid wing meningiomas involve the region of the anterior clinoid, adjacent medial sphenoid wing, superior orbital fissure, and cavernous sinus. They may grow into the orbit. As the tumor becomes larger, it may encase the internal carotid and proximal middle and anterior cerebral arteries. The optic nerve may be compressed or be surrounded by tumor. Large tumors put pressure on the frontal and temporal lobes and provoke edema in the adjacent brain tissue resulting in neurologic deficits or seizures.

Magnetic resonance imaging (MRI) outlines the extent of the tumor and shows the relationship to the arterial structures. It is often hard to define the optic nerves and chiasm. Angiography may be needed to determine the extent of encasement of the internal carotid artery and its branches and determines the blood supply to the tumor. Embollization of external carotid artery branches is occasionally indicated prior to operation.

The treatment decisions are often difficult because symptoms may be mild, the natural history is variable with some tumors having a very indolent course, the long-term results of microsurgical radical resections that have been proposed and the newer radiation therapy modalities (single dose radiosurgery or fractionated radiotherapy programs) are unknown.

However, some general guidelines for the treatment of these tumors can be outlined. For those with mild or non-progressive symptoms, it may be appropriate to follow the patient with periodic MRI and examination to determine if the lesion is growing and to see whether the symptoms are significantly interfering with the patient's life. The indications for surgery in younger patients are worsening symptoms and/or growth seen on follow-up scans, and in older patients a large tumor with worsening symptoms. Radiotherapy is used in older patients with small and medium

size tumors with worsening symptoms and for regrowth after subtotal or radical subtotal removal.

For most patients, a lateral subfrontal and anterior temporal exposure is used. Internal decompression of the tumor is done staying away from the region of the internal carotid and middle cerebral arteries. Some soft tumors can be more easily removed than very firm, hard tumors. The distal branches of the middle cerebral artery are identified and followed to the tumor capsule to determine if it is feasible to dissect them. In some situations arachnoid planes help in separating the tumor from and around the encased arteries. At some point, the relationship of the optic nerve and chiasm to the tumor is determined.
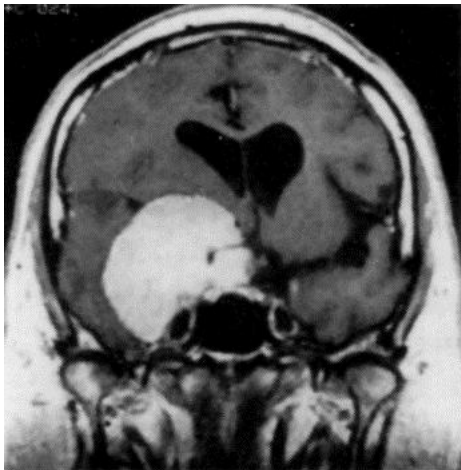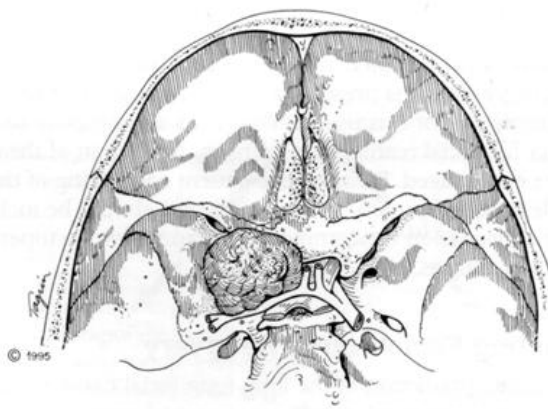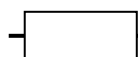


A
B

Figure 1. MRI Medial Sphenoid Wing Meningioma

This 57 year old man presented with worsening vision in the right eye and increasing dificulty with recent memory and judgement. On the T1 coronal image (A) with gadolinium enhancement the internal carotid and proxinial middle and anterior cerebral arteries are encased. The T2 axial image (B) shows marked edema in the surrounding brain. An extensive subtotal removal of the tumor was done and he made a good recovery except for residual visual loss in tha right eye.

Computed Tomography

Although no longer considered a standard for evaluation of the patient with epilepsy, CT is still useful in limited circumstances, notably when speed is paramount or when MRI is contraindicated. Compared to MRI, CT suffers from, by lesser soft tissue contrast, lack of multi-planar capability, and beam hardening artifacts at the skull base. Despite these limitations, CT readily depicts many of the pathologies which may underlie epilepsy, especially those associated with acute presentations such as hemorrhage, infarction, and mass lesions as well as obvious malformations and calcified lesions. Often CT serves as first line imaging in acute presentation where urgent treatment may be merited. Patients with hemispheric pathology such as Sturge-Weber or with calcified lesions found in tuberous sclerosis may be adequately evaluated with CT. Small tumors, subtle cortical malformations and mesial temporal sclerosis (MTS) may be easily missed with CT. In general patients with normal examinations or with lesions judged incompletely characterized by CT will then proceed to MRI.

MRI

Benefiting from superior soft tissue contrast, multi-planar capability, absence of bone artifact and potential for high resolution, MRI has evolved into the unrivaled imaging standard for routine evaluation of the epilepsy patient. Whereas CT imaging depicts one parameter, x-ray attenuation, MRI reflects a number of independent but related parameters relating to temporal dynamics of proton nuclei responding to changing magnetic fields. The parameters reflected in MRI include T1, T2,
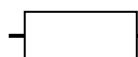
susceptibility effects (T2*) and proton density. Most MR sequences attempt to primarily demonstrate a single parameter although the resultant images are generally variably affected by others. Expansive MR development has yielded myriad imaging sequence approaches and options. The choice of optimal sequence and imaging plane depends upon suspected pathology and so is best done with clear communication between radiology and referring service following thorough clinical evaluation.

MRI protocols attempt to optimize two approaches to lesion detection. In the first, tissue contrast is maximized generally through T2 weighted imaging or related fluid attenuation inversion recovery (FLAIR) imaging. Such imaging increases sensitivity to lesions which exhibit T2 differences from normal brain, most notably MTS. In the second approach to imaging optimization, resolution is enhanced through use of thin slices, especially with 3D imaging acquisition which allows for reformatting in multiple planes. 3D thin slice imaging maximizes evaluation for subtle abnormalities which do not exhibit T2 changes, most notably MTS. In the second approach to imaging optimization, resolution is enhanced through use of thin slices, especially with 3D imaging acquisition which allows for reformatting in multiple planes. 3D thin slice imaging maximizes evaluation for subtle abnormalities which do not exhibit T2 changes, most notably cortical dysplasia. In this application, the 3D sequence parameters are chosen to augment signal intensity difference between grey and white matter, thereby improving visualization of structural abnormalities. Grey/white differentiation may also be enhanced using a T2 based sequence which includes a magnetization preparation pulse designed to increase tissue signal intensity differences. Sometimes referred to as "white matter inversion recovery" (WMIR), the sequence is similar to short tau inversion recovery (STIR). In STIR, an inversion recovery pulse is used to saturate fat through exploitation of its short T1 relative to other tissues. In WMIR,
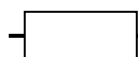
an inversion recovery pulse is used with a modified inversion time, arrived at empirically, to maximize signal intensity difference between the two tissues.

Example: RADIOLOGICAL DIAGNOSIS is meningioma of the sphenoid ridge, based on the broad implantation on the dura of the sphenoid bone with extraaxial location and the homogeneous enhancement.
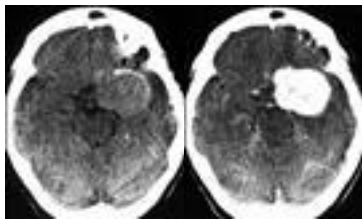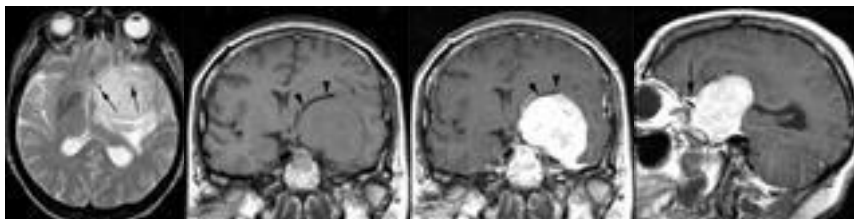

Fig. 1A (left), B (right)

Fig. 2A~E

Fig. 3

Fig. 1A NON-CONTRAST SCAN: Presence of a huge partially calcified (arrowheads) mass above the sphenoid ridge on the left side.

Fig. 1B CONTRAST-ENHANCED SCAN: Homogeneous contrast enhancement of the lesion.
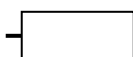
Fig. 2A TRANSAXIAL T2-WEIGHTED (2500/90/1) SPIN-ECHO SEQUENCE:
Confirmation of huge mass in the left deep frontotemporal region. The mass is in
close contact with the temporal bone and the sphenoid ridge. The lesion has an
overall slight hyperintense character, but with focal markedly hypointense signal
(arrows) due to calcification. Some edema is noted.

Fig. 2B CORONAL T1-WEIGHTED (640/20/1) SPIN-ECHO SEQUENCE: The
tumor is broadly implanted on the bone of the anterior temporal fossa and continues
along the cavernous sinus to the anterior cranial fossa. The middle cerebral artery is
markedly displaced upwards (arrowheads), together with the entire left temporal lobe
*and the Sylvian fissure (arrow). Note midline shift to the right.*

Fig. 2C CORONAL AND (2D) SAGITTAL GADOLINIUM- ENHANCED SPIN-
ECHO SEQUENCES: The tumor shows slightly inhomogeneous enhancement with
recognition of some radial patern of enhancement. A dural tail is seen along the
temporal bone (arrow). The tumor adheres to the cavernous sinus and continues over
the planum sphenoidale, where again a dural tail is noted (arrow). The right internal
carotid artery is severely compressed and narrowed by the tumor (arrow).
Furthermore the middle cerebral artery is elevated (arrowheads).

Fig. 3 ANGIOGRAPHY: selective left internal artery injection in the anteroposterior
projection: Narrowing of the supraclinoid portion of the right internal carotid artery.
Marked medial displacement of this portion. The left middle cerebral artery is
markedly displaced in an upward and posterior direction, and is narrowed. Note
tumor hypervascularity arising from ethmoidal branches of the ophthalmic artery and
temporal branches of the middle cerebral artery.

Mesial Temporal Sclerosis

The most common cause of complex partial seizures is mesial
temporal sclerosis, occurring in 35 to 65 percent of patients who undergo
temporal lobe surgery. In mesial temporal sclerosis, the hippocampus is
smaller than normal. This usually occurs on one side of the brain, but can
occur bilaterally in 10 to 15 percent of cases.

MRI detects mesial temporal sclerosis by demonstrating this size
asymmetry and abnormal signal within the atrophied hippocampus *(Fig.*
4A). Thin-section, high-resolution coronal MR images are best for
detecting these abnormalities, which can be subtle. T1-weighted images
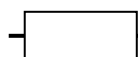
are best for detecting size asymmetry, and T2-weighted images are most sensitive for detecting signal changes. A special T2-weighted sequence called FLAIR (fluid attenuated inversion recovery) is even more sensitive for detecting signal abnormalities *(Fig.4B)*. With subtle hippocampal atrophy, quantitative three-dimensional volume measurements of each hippocampus can be useful. These volume measurements can be especially helpful when there is bilateral hippocampal atrophy.
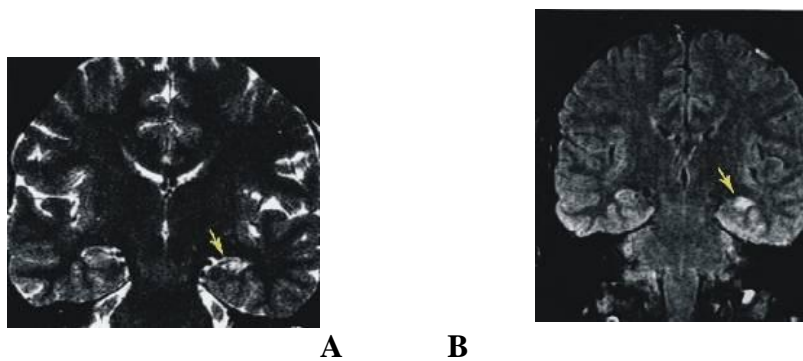

A B

Figure 4. (A) *MRI detects mesial temporal sclerosis by demonstrating this size asymmetry and abnormal signal within the atrophied hippocampus.* **(B)** Thin-section high-resolution coronal MR images are best for detecting these abnormalities, which can be subtle.

Epilepsy in childhood is most commonly due to structural changes in the brain that cannot be detected by any neuroradiological method. Most children with epilepsy will make a full recovery before adulthood. Malformations and destructive lesions of the brain can sometimes be associated with epilepsy and diagnostic efforts are often concentrated on identifying the se patients with the help of neuroradiology. Tumors of the brain are uncommon as the cause for epilepsy in childhood. It is neither practically possible, nor desirable to study all children with epilepsy using neuroradiological imaging methods. It is the task of the pediatric neurologist or pediatrician with specific expertise in neurology to select the patient who should be investigated using neuroradiology. It is important to recognize that a request for a neuroradiological investigation shall never replace a referral of the patient with epilepsy to a specialist in

pediatric neurology. The most commonly used criteria in selecting children suitable for CT examination of the brain are the following: (1) epilepsy with psycho-motor defects in a child below one year of age, particularly infantile spasm; (2) epilepsy with a changed seizure pattern - epilepsy with focal EEG-changes, particularly with focal slowing; (3) epilepsy with seizures resistant to medical therapy and in which surgery is contemplated; (4) status epilepticus; (5) post-traumatic epilepsy.

It is usually state d that the CT scanning can detect pathology in about 40 % of patients with infantile spasm. The diagnoses encountered include such diseases as phakomatoses, cerebral malformations or destructive brain damage that may have occurred in ufero or perinatally. If possible, this investigation should be delayed until the child has reached the age of six months, in order to maximize the diagnostic yield. It is easier to assess the structure of the brain at the age of six months and malformations are then easier to detect or exclude. Rare cases of a tumor causing epilepsy are found particularly in children with a changing pattern of epilepsy and in those with focal EEG-changes. The neuroradiological work-up is extensive, should surgery be contemplated as treatment for epilepsy. It will include MR-imaging, positron emission tomography and specialized neurophysiological methods (Fig. l). Positive findings are uncommon in patients with status epilepticus but the finding of a normal CT scan is quite helpful and important in the immediate care for the child that is unconscious following status epilepticus. Children developing seizures hours or days following a head trauma should be urgently investigated with a CT -scan, even if such a procedure was performed and found to be negative at the time of admission following the trauma. The possibility for delayed intracranial hemorrhage is significant in the short range, while development of leptomeningeal cysts is a distinct possibility in the long range.
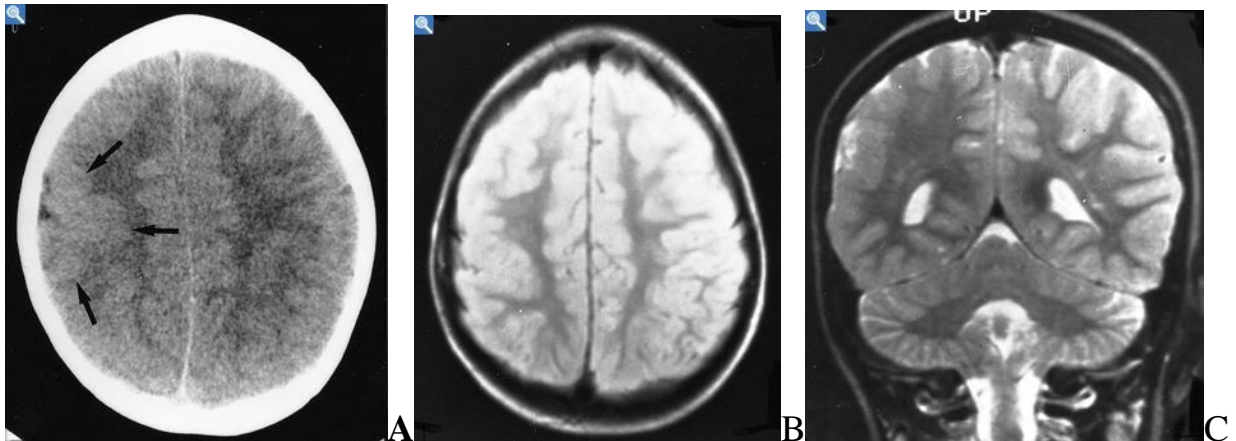
Figure 1.

This five-year-old boy has epilepsy with focal EEG-changes generated from the right cerebral hemisphere.

A) This CT-image through the parietal lobes shows a focal area in the right parietal region where the cortex has an abnormal appearance with thicker than usual cortical mantle (arrows). There is a widened sulcus superficial to this abnormality.
B) The corresponding MR proton weighted image shows the white matter in the right-sided centrum semiovale to lack the extensions normally found into each gyrus.
C) This heavily T2-weighted image in the coronal plane shows no abnormal signal characteristics but the rather simplistic pattern of white and gray matter in the right parietal lobe as compared to the left side. These images show a focal abnormality of neuronal migration following which the cortical structures have been malformed.

References:

http://www.medcyclopaedia.com/search.aspx?s=sphenoid+ridge&mode=1&scope=&syn=

（醫學系放射線學科・陳榮邦）